Equipment Calibration with a Laser Interruption Sensor

Yan-Hong Lu, Yu-Wei Lin, Sheng-Chieh Hsu, Tien-Yun Chi, Yu-Hsiu Lee

***Abstract*—This paper introduces a novel method for equipment calibration using a customized actuated laser cross-beam sensor, addressing the tool center point (TCP) calibration challenge in robot manipulators used in the automation industry. Unlike existing methods which are often complex and expensive, our approach effectively integrates TCP calibration with equipment calibration, utilizing the least possible robot movements for enhanced speed and cost-effectiveness. Our approach has been tested through both simulations and actual experiments, yielding calibration precision of 0.078 mm and 0.060 mm, respectively. The high accuracy underscores the potential of our calibration method to improve robotic manipulation in industrial applications.**

Index Terms*—*Automated Calibration, Equipment Calibration, Laser Interruption Sensor, Robot Manipulator, Tool Center Point (TCP) Calibration

I. Introduction

ROBOT manipulators are widely used in automation industry for their flexibility. Since different tools will be mounted for different processes [1], an economical and effective tool center point (TCP) calibration method is necessary [2]. In addition to TCP calibration, the equipment used for TCP calibration itself must also be calibrated relative to the robot's coordinate system before use. Common techniques for TCP calibration include vision-based calibration, laser tracker systems, interruption-type laser cross-beam sensor [3], etc. Liu et al. (2021) present an innovative automatic calibration algorithm for robots' Tool Center Point (TCP) utilizing binocular vision [4]. Zhang et al. (2017) introduce a novel approach to autonomous robot calibration using stereo vision, significantly improving robotic systems' self-calibration capabilities [5]. Moeller et al. (2017) explore the implementation of real-time pose control in industrial robotic systems for machining large-scale aerospace components, demonstrating enhanced accuracy through the use of a laser tracker system [6]. Aalamifar et al. (2016) developed a framework for automatic ultrasound calibration with robot assistance, eliminating the need for temporal calibration and reducing calibration time by 58% compared to manual methods [7].

Although numerous methods for TCP calibration exist, they are often complex or expensive. Laser cross-beam sensors find a good compromise between equipment cost and accuracy [8]-[11]. For instance, Konolige et al. (2008) developed a compact laser distance sensor offering comparable capabilities to laser scanners at that time at a significantly lower cost, highlighting the cost-effectiveness of laser-based sensing technologies for consumer robot platforms [8]. The conventional approach installs the tool calibration equipment with a known relationship with respect to the robot inertial frame so that the TCP offset can be obtained [12][13]. However, they less frequently address the calibration of the equipment itself. The setup for the calibration equipment can be costly and time-consuming [14]-[17].

Therefore, this study developed a novel equipment calibration method using a customized actuated laser cross-beam sensor. The features of this calibration method are:

1. It simultaneously accomplishes TCP calibration while calibrating the coordinate systems between the robot and the equipment.
2. It utilizes the least possible robot movements, ensuring both speed and cost-effectiveness.

The structure of this paper initially defines the problem in mathematical terms, then progressively introduces the calibration algorithm developed in this study. Finally, the effectiveness of the algorithm is validated through simulations and actual experiments, with the calibration accuracy being quantified. For convenience, TABLE I represents the nomenclature of this paper.

TABLE I
NOMENCLATURE OF THIS PAPER

Notation	Definition
B	Base of the robotic arm
F	Flange of the robotic arm
R	Intersection point of the cross-beam lasers
S	Base of the laser cross-beam sensor
$\{B\}$	Coordinate frame B
H_S^B	Homogeneous transformation matrix, $\{S\}$ relative to $\{B\}$
R_S^B	Rotation matrix, $\{S\}$ relative to $\{B\}$
Y^{-1}, Y^T	Matrix Y inverse and transpose
p_S^B	Position vector, $\{S\}$ relative to $\{B\}$
t^B	Vector t in coordinate frame $\{B\}$
${t_x}^B$	x component of t^B
Δt^B	Difference of t^B
$\|\Delta t^B\|$	Magnitude of Δt^B
δ	Measurement error of the laser cross-beam sensor
α, β, γ	Euler angles (unit: deg)

II. Problem Formulation

The equipment calibration problem can be visualized as shown in Fig. 1, featuring a six-axis robotic arm and a customized actuated laser cross-beam sensor. The sensor is equipped with a pair of intersecting laser beams and a circular

Manuscript received 23 April 2024; received in the revised form 14 June 2024; accepted 16 June 2024; Date of publication 25 June 2024. This research is supported by the Industrial Technology Research Institute in Taiwan.

Yan-Hong Lu, Yu-Wei Lin, and Yu-Hsiu Lee (corresponding author) are with the National Taiwan University, Taipei 106319, Taiwan (phone: 886-2-3366-2715; e-mail: yuhsiulee@ntu.edu.tw).

Sheng-Chieh Hsu and Tien-Yun Chi are with the Industrial Technology Research Institute (ITRI), Hsinchu, Taiwan.

sensing area with a 210 mm diameter, possessing three translational degrees of freedom (DOF) and a rotational DOF perpendicular to the ground. We employ Denavit-Hartenberg parameters [18] to construct homogeneous transformation matrices for coordinate transformation. maps the robot base $\{B\}$ to the robot flange $\{F\}$, H_R^S maps the sensor base $\{S\}$ to the intersection point of the cross-beam lasers $\{R\}$, and so forth. It is assumed that H_F^B and H_R^S are known, and the movements of both devices are error-free. However, the laser beams exhibit a 0.03 mm error.

The goal is to determine the homogeneous transformation matrix H_S^B for equipment calibration when a tool with an unknown offset t^B with respect to $\{B\}$ is mounted on the flange. H_S^B encompasses a rotation matrix R_S^B and a position vector p_S^B. This is accomplished through a series of designated robot movements and the interruption signals observed from the laser cross-beam sensor.

In summary, the objective and conditions of this study are as follows:

- The objective is to determine the unknown H_S^B.
- H_F^B and H_R^S are known.
- t^B is unknown.
- The movements of the robot and the sensor are error-free.
- The sensor has a measurement error of 0.03 mm.

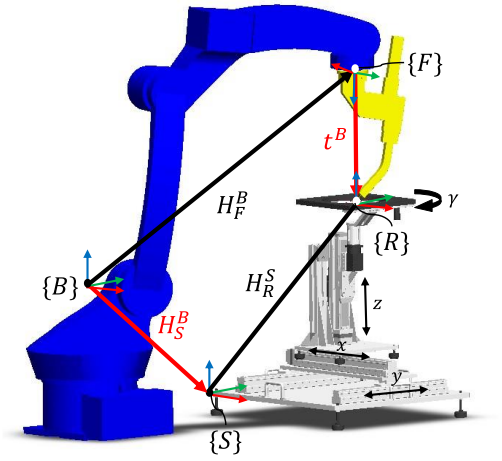

Fig. 1. Relationship between the robot and the laser cross-beam sensor

III. Methodology

This study introduces an algorithm for equipment calibration as shown in Fig. 2. The process can be divided into two stages. The first stage calibrates three Euler angles (denoted as α, β, γ, as illustrated in Fig. 3) of R_S^B by comparing the robot translational motion and the projected components in the sensor coordinate. In the second stage, the tool offset t^B is computed. Once t^B is found, p_S^B can be determined using vector algebra from the closed-loop configuration shown in Fig. 1.

Throughout the equipment calibration process, the laser cross-beam sensor repetitively utilizes its four-axis motion to locate the tool center point (TCP). To prevent collision between the two devices, the sensor's planar translation in any direction is limited to a quarter of the sensing range's diameter, i.e., ±52.5 mm. Additionally, the TCP must remain within the circle that has a diameter half that of the sensing area, which can be determined by the interruption signal's duration when the sensor rotates at a constant speed, as illustrated in Fig. 4. The TCP's position is determined by initially employing the bisection method to identify the tool's lowest point, followed by scanning the tool from both horizontal axes, as depicted in Fig. 5. By selecting the midpoint of the interruption signal, the TCP's planar position is determined.

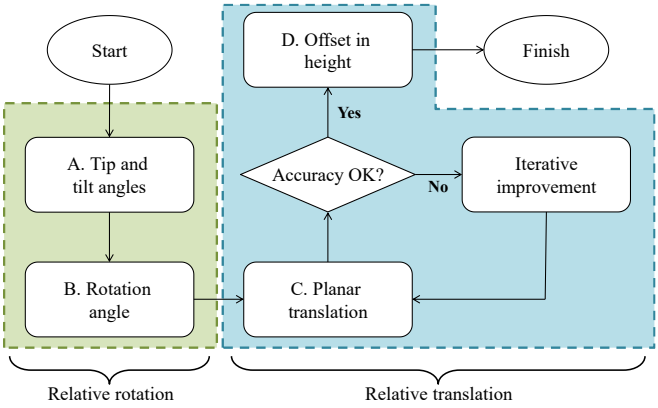

Fig. 2. Equipment calibration process

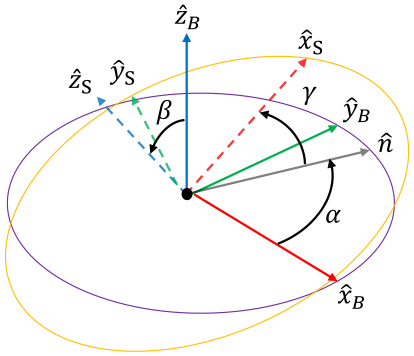

Fig. 3. Euler angles α, β, γ, where axis $\hat{n}$ is defined as the common perpendicular to the axes $\hat{z}_B$ and $\hat{z}_S$

A. Tip and tilt angles

As shown in Fig. 6, to determine the tip angle α and tilt angle β, the robot moves $\{F\}$ along an arbitrary vector v^B that lies on the xz-plane or yz-plane of $\{B\}$, and the sensor measures the TCP's displacement as vector v^S. By decomposing these vectors, i.e., $v^B = \begin{bmatrix} {v_x}^B & {v_y}^B & {v_z}^B \end{bmatrix}^T$, $v^S = \begin{bmatrix} {v_x}^S & {v_y}^S & {v_z}^S \end{bmatrix}^T$, α and β can be determined using trigonometric functions (1) and (2), where $0° \le \alpha \le 360°$, $0° \le \beta \le 90°$.

$$\alpha = \tan^{-1}\left(\frac{{v_y}^S}{{v_x}^S}\right) \quad (1)$$

$$\beta = \tan^{-1}\left(\frac{{v_z}^S}{\left\|\begin{bmatrix} {v_y}^S & {v_x}^S \end{bmatrix}^T\right\|}\right) - \tan^{-1}\left(\frac{{v_z}^B}{\left\|\begin{bmatrix} {v_y}^B & {v_x}^B \end{bmatrix}^T\right\|}\right) \quad (2)$$

To minimize the impact of the 0.03 mm error of the laser beams (denoted as δ), we intentionally move the robot along a planar vector rather than a simpler axial vector. Equations after considering the errors are shown in (3)-(5). For instance, if the

TCP moves along the z-axis, considering normal cases that the relative rotation before calibration is not expected to be significant, e.g., $\alpha, \beta \sim 1°$, both ${v_x}^S$ and ${v_y}^S$ would be minimal. Hence, α is significantly affected by δ_1 and δ_2, whereas β, due to the relative large ${v_z}^S$, is less impacted by the errors. Thus, choosing an arbitrary planar vector increases either ${v_x}^S$ or ${v_y}^S$, reducing the error's impact on α.

$$-0.015 \le \delta \le 0.015,\ \delta \in [\delta_1 \quad \delta_2 \quad \delta_3]^T \tag{3}$$

$$\alpha = \tan^{-1}\left(\frac{{v_y}^S+\delta_2}{{v_x}^S+\delta_1}\right) \tag{4}$$

$$\beta = \tan^{-1}\left(\frac{{v_z}^S+\delta_3}{\|[{v_y}^S+\delta_2 \quad {v_x}^S+\delta_1]^T\|}\right) - \tan^{-1}\left(\frac{{v_z}^B}{\|[{v_y}^B \quad {v_x}^B]^T\|}\right) \tag{5}$$

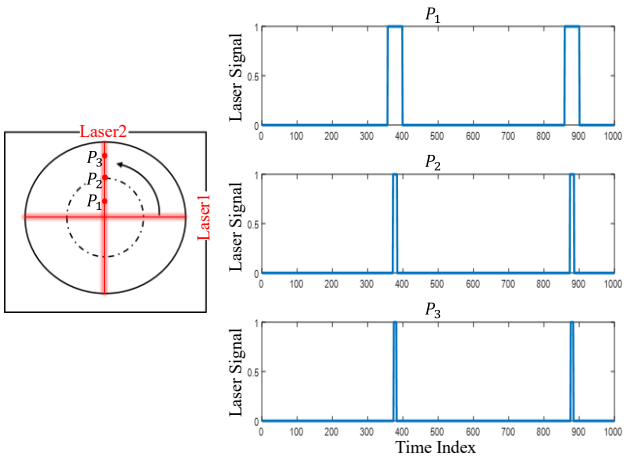

Fig. 4. When the sensor rotates at a constant speed, the interruption signal's duration P_x varies depending on the TCP's position due to the fixed width of the laser beam (i.e., $P_1 > P_2 > P_3$)

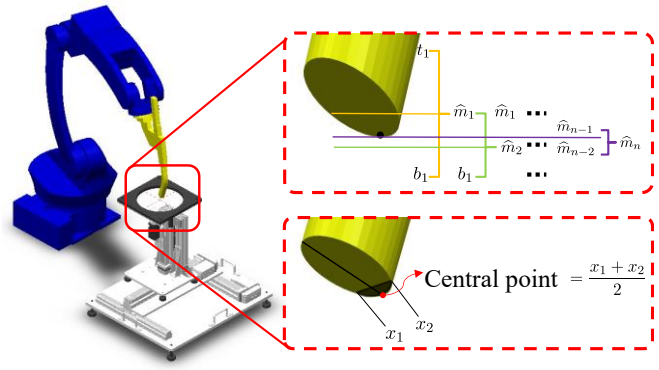

Fig. 5. Locating TCP's lowest point and its planar position

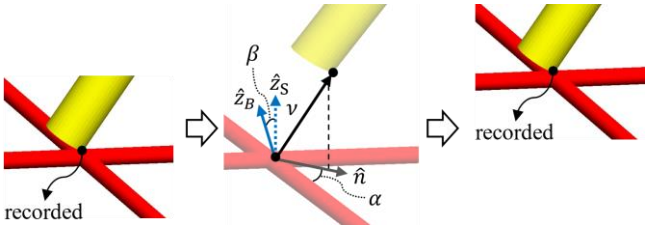

Fig. 6. Determining the tip angle α and tilt angle β

B. *Rotation angle*

The method for determining the rotation angle γ is similar to that for determining angles α and β, as shown in Fig. 7. After calibrating the tip and tilt angles, i.e., $\alpha, \beta = 0°$, the robot moves $\{F\}$ along an vector w^B on the x-axis or y-axis of $\{B\}$, and the sensor measures the TCP's displacement as vector w^S with respect to $\{S\}$. By decomposing these vectors, i.e., $w^S = [{w_x}^S \quad {w_y}^S \quad {w_z}^S]^T$, γ can be determined using (6), where $0° \le \gamma \le 90°$.

$$\gamma = \tan^{-1}\left(\frac{{w_y}^S}{{w_x}^S}\right) \tag{6}$$

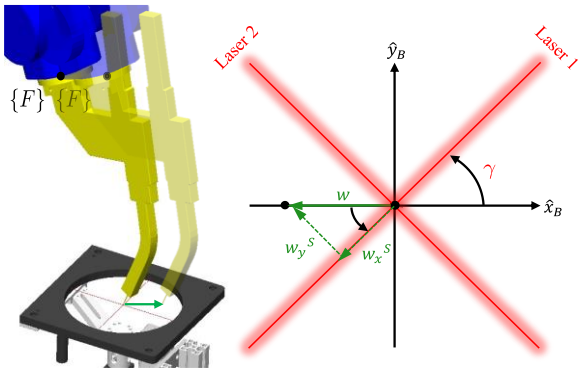

Fig. 7. Determining the rotation angle γ

C. *Planar translation*

The following steps of the calibration of planar translation and offset in height are done after the calibration of the Euler angles. The planar translation of t^B, i.e., ${t_x}^B$ and ${t_y}^B$, is determined in this step, as shown in Fig. 8. After the calibration of the Euler angles, the robot rotates $\{F\}$ around an axis that intersects the origin of $\{F\}$ and is parallel to the z-axis of $\{B\}$, causing the TCP to trace a circular arc trajectory. Throughout this movement, the sensor records multiple planar coordinates (x_j, y_j) of the TCP, where $j = 1,2,3,\dots n$. This study utilized these coordinates to derive the center of the arc (x_c, y_c) using least squares fitting [19]. Equation (7) is the general form of a plane circle, where c_1, c_2, and c_3 are constants that are determined using (8) and (9). (x_c, y_c) and the radius of the arc R can then be computed using (7), as listed in (10). Noted that x_c and y_c can be expressed as vectors with respect to $\{S\}$, i.e., ${x_c}^S$ and ${y_c}^S$. These are transformed to ${x_c}^R$ and ${y_c}^R$ using H_R^S. When the TCP aligns with the origin of $\{R\}$, ${t_x}^B$ and ${t_y}^B$ are obtained as ${t_x}^B = -{x_c}^R$ and ${t_y}^B = -{y_c}^R$, respectively.

$${x_j}^2 + {y_j}^2 + c_1 x_j + c_2 y_j + c_3 = 0 \tag{7}$$

$$X = (Y^T Y)^{-1} Y^T Z \tag{8}$$

$$X = \begin{bmatrix} c_1 \\ c_2 \\ c_3 \end{bmatrix}, Y = \begin{bmatrix} x_1 & y_1 & 1 \\ & \vdots & \\ x_n & y_n & 1 \end{bmatrix}, Z = \begin{bmatrix} -({x_1}^2 + {y_1}^2) \\ \vdots \\ -({x_n}^2 + {y_n}^2) \end{bmatrix} \tag{9}$$

$$x_c = -\frac{c_1}{2},\ y_c = -\frac{c_2}{2},\ R = \sqrt{\frac{{c_1}^2+{c_2}^2-4c_3}{4}} \tag{10}$$

However, subsequent simulations have revealed that errors in ${t_x}^B$ and ${t_y}^B$ can reach up to 1.22 mm. A plausible explanation is the initial planar position of $\{F\}$, i.e., (x_c, y_c), being distant from the origin of $\{R\}$, which leads to a small rotation angle of the TCP due to the limited sensing range. The smaller rotation

angle results in a more constrained distribution of (x_j, y_j) across the entire circle, which potentially undermining the accuracy of the fitting outcomes [20], as illustrated in Fig. 9. To address this issue, our research introduces an iterative method to increase the rotation angle and improve the fitting accuracy, as illustrated in Fig. 10. After the initial calculation of ${t_x}^B$ and ${t_y}^B$, the robot moves $\{F\}$ to make the planar translation zero, i.e., ${t_x}^B = 0$ and ${t_y}^B = 0$, and then repeat the process of determining the planar translation. Despite substantial errors in the initial ${t_x}^B$ and ${t_y}^B$, iteration can greatly reduce the planar distance between $\{F\}$ and $\{R\}$, increase the rotation angle, and thus reduce the error in the circle fitting algorithm. Subsequent simulations and experiments have confirmed the effectiveness of this iterative method.

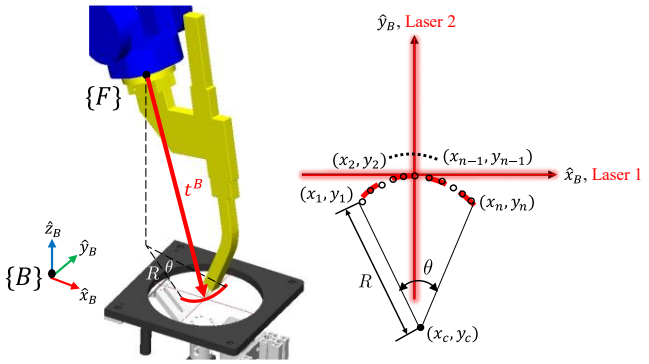

Fig. 8. Determining the planar translation of t^B with respect to $\{S\}$ by least squares fitting [19]

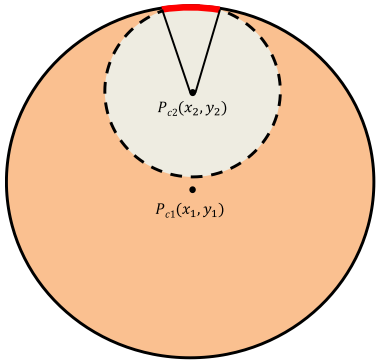

Fig. 9. A small circular arc trajectory of the TCP (the red section). Under the influence of measurement errors from the laser sensor, the calculated centor of the circle (x_c, y_c) could potentially be either P_{c1} or P_{c2}, resulting in significant error

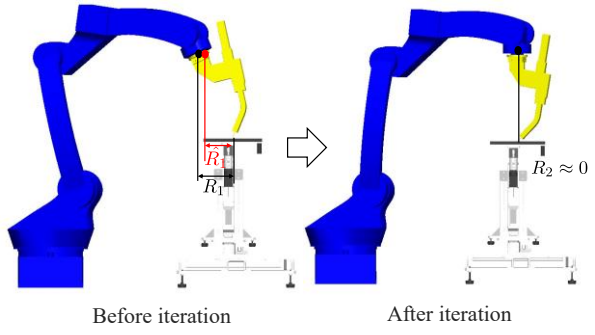

Fig. 10. The initially computed radius, $\hat{R}_1$, may exhibit a large bias relative to the theoretical value R_1. As R_2 decreases following the iterative process, the rotation angle increases, thereby enhancing the calculation accuracy

D. Offset in height

The tool offset in height, i.e., ${t_z}^B$, is computed based on the premise that both the robot and the sensor share a common plane, as shown in Fig. 11. Knowing the heights of $\{F\}$ and $\{R\}$, the value of ${t_z}^B$ is derived through subtraction.

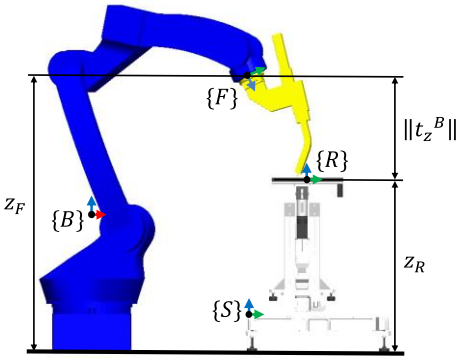

Fig. 11. Determining the tool offset in height ${t_z}^F$ assuming that both devices share a common plane

IV. Simulation

In this research, MATLAB simulations were conducted for equipment calibration, with the assumption that the laser beams' 0.03 mm error follows a normal distribution. After specifying reasonable theoretical values for Euler angles and t^B, the simulation results are shown in TABLE II and TABLE III. TABLE II shows errors in tip and tilt angles under 0.004 degrees and in rotation angle 0.308 degrees, validating the accuracy of the proposed Euler angle calibration approach. TABLE III shows the simulation results of computing t^B, noting that before iteration, the error in planar translation reached up to 1.22 mm. However, following a single iteration, the errors in planar translation were significantly reduced to 0.024 mm.

TABLE II
Simulation Results of Euler Angle Calibration (Unit: Degree)

	Theoretical Values	**Simulated Values**	**Errors**
α	0.05	0.054	0.004
β	0.08	0.082	0.002
γ	30	29.692	-0.308

TABLE III
Simulation Results of Tool Offset Calibration (Unit: mm)

Before iteration			
	Theoretical Value	**Simulated Value**	**Error**
${t_x}^B$	188.426	189.649	1.223
${t_y}^B$	233.443	234.636	1.193
${t_z}^B$	-288.541	-288.496	0.045
$\|\Delta t^B\|$	-	-	1.709
After iteration			
	Theoretical Value	**Simulated Value**	**Error**
${t_x}^B$	-1.223	-1.207	0.016
${t_y}^B$	-1.193	-1.169	0.024
${t_z}^B$	-416.237	-416.165	0.072
$\|\Delta t^B\|$	-	-	0.078

In the calibration of tool's planar translation, excessive errors can potentially lead to collisions during iterative process. To address this, our study conducted simulations of planar translation steps 50,000 times each for different theoretical values of R and the corresponding maximum possible rotation angles, as illustrated in Fig. 12. Samples from each set of 50,000 simulations, i.e., the green data, show that nearly all samples are within 3 standard deviations, consistent with the empirical rule. This indicates that the error margins of planar translation can be predicted through the empirical rule, allowing for a corresponding reduction in sensor height prior to the iterative process to avoid collisions.

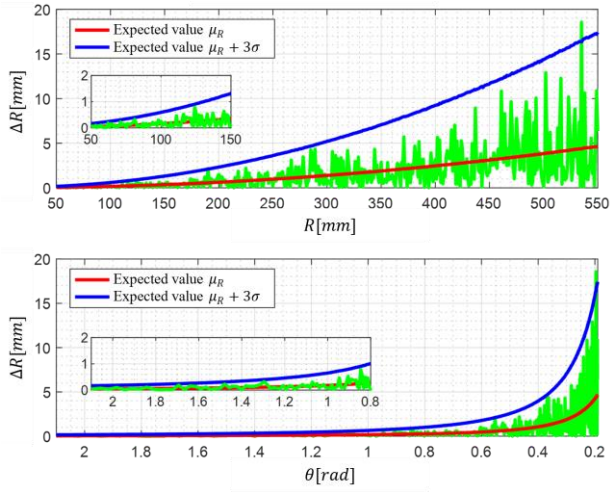

Fig. 12. The error margins of planar translation are consistent with the empirical rule in the simulation environment

V. Experiment

In the practical experiments, a YASKAWA MOTOMAN-GP12 robot was employed, coupled with the customized laser sensor. One difference from the methodology was that there was an immovable block beneath the robot due to environmental setup constraints. Without the precise specifications of this block, the original method for determining tool offset in height could not be applied. Consequently, this study utilized a reference tool with known height mounted on the flange to calibrate the offset in height.

This study designed an experiment to validate the effectiveness of the least squares fitting and the iterative approach in the calibration process of planar translation, as shown in Fig. 13. In the experiment, the calibration process of planar translation was conducted with three different flange inclinations θ_F, i.e., different magnitude of the tool's planar offset, to simulate the iteration process. The errors between the experimental and theoretical values of the tool offset were recorded as shown in Fig. 14. It was observed that lower values of θ_F, i.e., smaller tool's planar offset, yielded more precise calibrations, with $\|\Delta t^B\|$ being reduced to less than 0.060 mm in the experiment. The results show that the iterative approach can increase the accuracy of the circle fitting algorithm.

In the experiment, it is noteworthy that $\|\Delta t^B\|$ is smaller by 0.018 mm compared to that in the simulation. This study proposes two potential reasons for this difference. Firstly, the difference falls within the measurement error range of the laser sensor, which is 0.03mm. Secondly, the experiment has focused only on the calibration of relative translation, with relative rotation being manually calibrated using external instruments in the first place. In contrast, in the simulation, the calibration of relative rotation is performed before the calibration of relative translation, implying that errors in the calibration of relative rotation may impact the results of relative translation. This difference could explain why $\|\Delta t^B\|$ in the simulation is larger than that in the experiment.

Finally, this study implemented a complete equipment calibration process using a tool with an unknown vector. After the calibration, the robot moved around with the position of the TCP being fixed, as demonstrated in Fig. 15.

Fig. 13. Experiment of the planar translation calibration by varying the flange inclinations θ_F

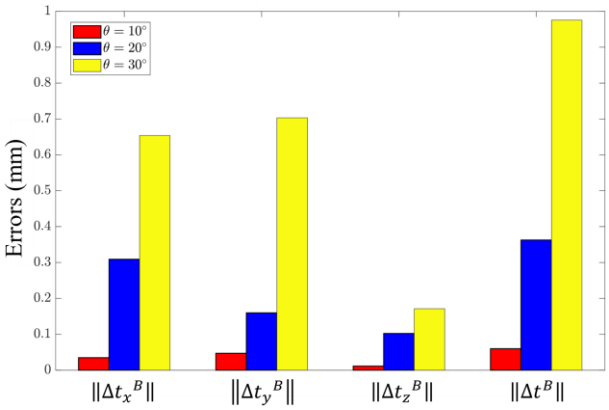

Fig. 14. Experiment results of planar translation calibration

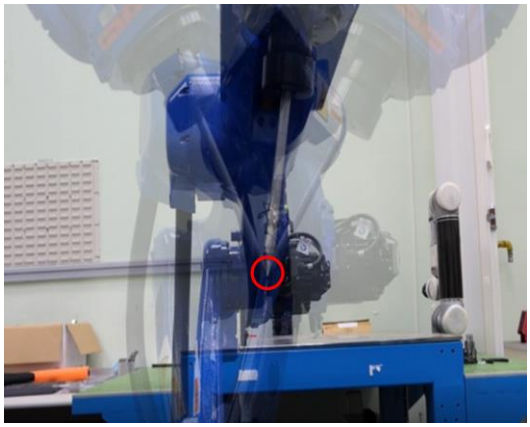

Fig. 15. Demonstration after the whole equipment calibration process

VI. Conclusion

This study designed an experiment to validate the effectiveness of the least squares fitting and the iterative approach in the calibration process of planar translation, as shown in Fig. 13. In the experiment, the calibration process of planar translation was conducted with three different flange inclinations θ_F, i.e., different magnitude of the tool's planar offset, to simulate the iteration process. The errors between the experimental and theoretical values of the tool offset were recorded as shown in Fig. 14. It was observed that lower values of θ_F, i.e., smaller tool's planar offset, yielded more precise calibrations, with $\|\Delta t^B\|$ being reduced to less than 0.060 mm in the experiment. The results show that the iterative approach can increase the accuracy of the circle fitting algorithm.

References

[1] Brogårdh, T. (2007). Present and future robot control development—An industrial perspective. *Annual Reviews in Control*, *31*(1), 69-79.

[2] Li, Z., Li, S., & Luo, X. (2021). An overview of calibration technology of industrial robots. *IEEE/CAA Journal of Automatica Sinica*, *8*(1), 23-36.

[3] LEONI Advintec Solution, Leoni, Inc. https://www.leoni-serbia.com/en/press/releases/details/automate-2022-robot-tool-calibration-system/

[4] Liu, S., Wu, Y., Qiu, C., & Zou, X. (2021, August). Automatic calibration algorithm of robot TCP based on binocular vision. In *Proceedings of the 2021 2nd International Conference on Control, Robotics and Intelligent System* (pp. 244-249).

[5] Zhang, X., Song, Y., Yang, Y., & Pan, H. (2017). Stereo vision based autonomous robot calibration. *Robotics and Autonomous Systems*, *93*, 43-51.

[6] Moeller, C., Schmidt, H. C., Koch, P., Boehlmann, C., Kothe, S., Wollnack, J., & Hintze, W. (2017). Real time pose control of an industrial robotic system for machining of large scale components in aerospace industry using laser tracker system. *SAE International journal of aerospace*, *10*(2), 100-108.

[7] Aalamifar, F., Cheng, A., Kim, Y., Hu, X., Zhang, H. K., Guo, X., & Boctor, E. M. (2016). Robot-assisted automatic ultrasound calibration. *International journal of computer assisted radiology and surgery*, *11*, 1821-1829.

[8] Konolige, K., Augenbraun, J., Donaldson, N., Fiebig, C., & Shah, P. (2008). A low-cost laser distance sensor. *2008 IEEE International Conference on Robotics and Automation*, 3002-3008. https://doi.org/10.1109/ROBOT.2008.4543666.

[9] Kang, J., Wu, B., & Xue, T. (2019). Articulated laser sensor for three-dimensional precision measurement. *IEEE access*, *7*, 121255-121264.

[10] Gao, J., & Peh, L. (2016). A smartphone-based laser distance sensor for outdoor environments. *2016 IEEE International Conference on Robotics and Automation (ICRA)*, 2922-2929. https://doi.org/10.1109/ICRA.2016.7487457.

[11] Kim, Y., Kim, Y., Jung, Y., Jang, I., Kim, K., Kim, S., & Kwak, B. (2013). Developing Accurate Long-Distance 6-DOF Motion Detection With One-Dimensional Laser Sensors: Three-Beam Detection System. *IEEE Transactions on Industrial Electronics*, 60, 3386-3395. https://doi.org/10.1109/TIE.2012.2200225.

[12] Liska, J., Chalus, M., & Vanicek, O. (2018, August). Iterative refinement of hand-eye calibration. In *2018 IEEE 14th International Conference on Automation Science and Engineering (CASE)* (pp. 457-462). IEEE.

[13] Liska, J., Vanicek, O., & Chalus, M. (2018, July). Hand-eye calibration of a laser profile scanner in robotic welding. In *2018 IEEE/ASME International Conference on Advanced Intelligent Mechatronics (AIM)* (pp. 316-321). IEEE.

[14] Du, G., & Zhang, P. (2013). Online robot calibration based on vision measurement. *Robotics and Computer-integrated Manufacturing*, 29, 484-492. https://doi.org/10.1016/J.RCIM.2013.05.003.

[15] Gaudreault, M., Joubair, A., & Bonev, I. (2018). Self-Calibration of an Industrial Robot Using a Novel Affordable 3D Measuring Device. *Sensors (Basel, Switzerland)*, 18. https://doi.org/10.3390/s18103380.

[16] Beyer, L., & Wulfsberg, J. (2004). Practical robot calibration with ROSY. *Robotica*, 22, 505 - 512. https://doi.org/10.1017/S026357470400027X.

[17] Robinson, P., Orzechowski, P., James, P., & Smith, C. (1997). An automated robot calibration system. *ISIE '97 Proceeding of the IEEE International Symposium on Industrial Electronics*, 1, SS285-SS290 vol.1. https://doi.org/10.1109/ISIE.1997.651777.

[18] Denavit, J., & Hartenberg, R. S. (1955). A kinematic notation for lower-pair mechanisms based on matrices. *Journal of Applied Mechanics*, *22*(2), 215–221. https://doi.org/10.1115/1.4011045

[19] Al-Sharadqah, A., & Chernov, N. (2009). Error analysis for circle fitting algorithms. *Electronic Journal of Statistics*, 3(none). https://doi.org/10.1214/09-ejs419

[20] Herman, M., & Somlo, P. I. (1986). Efficient procedures for fitting circles and ellipses with application to sliding termination measurements. *IEEE transactions on instrumentation and measurement*, (1), 31-35.

Yan-Hong Lu received the B.S. degree in Mechanical Engineering from National Taiwan University, Taipei, Taiwan, and the M.S. degree in Mechanical Engineering from Mechatronics and Robotic Systems Laboratory, National Taiwan University, Taipei, Taiwan, in 2023.

Yu-Wei Lin is an incoming M.S. student in Mechanical Engineering at Stanford University, Stanford, CA, USA. He received the B.S. degree in Mechanical Engineering from National Taiwan University, Taipei, Taiwan, in 2024. He is interested in robotic systems development, mechanical design, and machine learning.

Sheng-Chieh Hsu received the B.S. degree in Aeronautics and Astronautics from National Cheng Kung University, Tainan, Taiwan, in 2015, and the M.S. degree in Power Mechanical Engineering from National Tsing Hua University, Hsinchu, Taiwan, in 2017. He is an engineer from Mechanical and Mechatronic Systems Laboratories of Industrial Technology Research Institute (ITRI). His research interests include robot calibration and industrial automation.

Tien-Yun Chi received the B.S. degree in Mechanical Engineering from National Cheng Kung University, Tainan, Taiwan, in 2007, and the M.S. degree in Mechanical Engineering from National Chiao Tung University, Hsinchu, Taiwan, in 2009. He is an engineer from Mechanical and Mechatronic Systems Laboratories of Industrial Technology Research Institute (ITRI). His research interests include robotics, simulation, and industrial automation.

Yu-Hsiu Lee received the Ph.D. degree in mechanical engineering from the University of California, Los Angeles, CA, USE, in 2019. He is currently an Assistant Professor of Mechanical Engineering, National Taiwan University, Taipei, Taiwan. His research interests include medical robotics, image-guided intervention, and inversion-based control methods.